

# Galactic diffuse gamma-ray flux at the energy about 175 TeV

Romen M. Martirosov\*, Samvel V. Ter-Antonyan†, Anatoly D. Erlykin‡, Alexandr P. Garyaka\*,  
Natalya M. Nikolskaya‡, Yves A. Gallant§ and Lawrence W. Jones¶

\*Yerevan Physics Institute, Yerevan, Armenia

†Department of Physics, Southern University, Baton Rouge, LA, USA

‡Russian Academy of Sciences, Lebedev Physical Institute, Moscow, Russia

§Lab. de Physique Theorique et Astroparticules, Universite Montpellier II, Montpellier, FRANCE

¶Department of Physics, University of Michigan, Ann Arbor, USA

**Abstract.** We present an upper limit of galactic diffuse gamma-ray flux, measured with the GAMMA experiment at energy about 175 TeV. The results were obtained using selection of muon poor extensive air showers at mountain level (700 g/cm<sup>2</sup>, Mt. Aragats, Armenia) for 5 GeV muon energy threshold. An upper limit for the differential flux at energy  $E_\gamma \simeq 175_{-20}^{+25}$  TeV is equal to  $(5.8 - 7.0) \cdot 10^{-12}$  (erg · m<sup>2</sup> · s · sr)<sup>-1</sup> for 95% confidence level<sup>1</sup>.

**Keywords:** Cosmic rays, gamma ray, energy spectrum

## I. INTRODUCTION

Ultra-high energy ( $E > 100$  TeV) galactic gamma-radiation is an important source of information about the origin of cosmic rays and their propagation. According to conventional model of cosmic rays the expected flux of ultra-high energy  $\gamma$ -rays in the energy range of 0.1 – 1 PeV has presumably to have hadronic origin from sources distributed within radii  $\sim 1 - 0.01$  Mpc [1] respectively.

In the very-high (TeV) energy region  $\gamma$ -ray flux was measured by ground-based systems and single Cherenkov telescopes (Whipple [2], CANGAROO [3], MAGIC [4], H.E.S.S. [5], MILAGRO [6]). The measurements in the ultra-high energy region ( $E > 100$  TeV) are still poor and made only by extensive air showers (EAS) arrays at Chacaltaya [7], MSU [8], Tien-Shan [9], CASA-MIA [11], EAS-TOP [12], KASCADE [13] and Grapes-III [10].

This paper is devoted to measurements of the diffuse gamma-rays with GAMMA EAS array [14], [15] at Aragats mountain observatory, where correlation of observable shower parameters with primary energy is about 0.98. The primary nuclei (predominantly  $H$ ) and  $\gamma$ -showers were discriminated using no-muon signal from underground muon scintillation carpet.

## II. GAMMA EXPERIMENT

GAMMA experiment [14], [15] is the ongoing study of primary energy spectra in the range of  $10^{14} - 10^{17}$

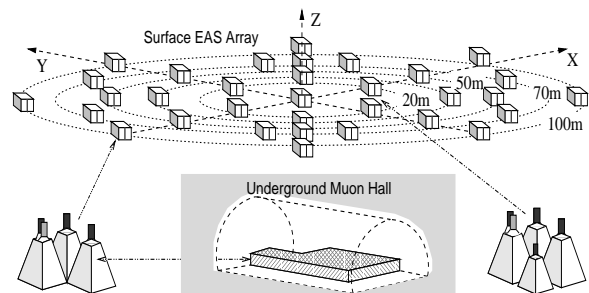


Fig. 1. Layout of GAMMA experiment.

eV using EAS array with 33 concentric disposed scintillator stations (each of  $3 \times 1 \text{m}^2$ ) and underground scintillation carpet with 150 scintillators (each of  $1 \text{m}^2$ ) to detect the shower muon component with energy  $E_\mu > 5 \text{GeV} / \cos \theta$ , where  $\theta$  is the shower zenith angle. Layout of GAMMA facility is presented in Fig. 1.

The detailed description of experiment, results of exploration of  $p$ ,  $He$ ,  $O$ -like, and  $Fe$ -like primary nuclei energy spectra derived from parametrized EAS inverse problem solution are presented in [14]. The all-particle primary energy spectrum obtained from event-by-event analysis is published in [15].

Here, the discrimination of  $\gamma$ -showers from primary nuclei induced showers is performed on the basis of following 6 conditions:

- 1) the reconstructed shower core coordinates is distributed within radius of  $R < 15 \text{m}$ ;
- 2) shower zenith angles  $\theta < 30^\circ$ ;
- 3) reconstructed shower size  $N_{ch} > 10^5$ ;
- 4) reconstructed shower age parameters ( $s$ ) is distributed within  $0.4 < s < 1.5$ ;
- 5) goodness-of-fit test for reconstructed showers  $\chi^2 < 2.5$ ;
- 6) no-muon signal is recorded for detected showers satisfying the previous 5 conditions.

The selection criteria and  $\gamma$ -shower discrimination rule (6) above were obtained using CORSIKA shower simulation code [16] for the NKG and EGS modes in the frameworks of the SIBYLL [17] interaction model. Simulations were done for 4 nuclear species:  $p$ ,  $He$ ,  $O$ ,  $Fe$  using united energy spectral index

<sup>1</sup>Corresponding author:

E-mail: samvel\_terantonyan@subr.edu (S.V. Ter-Antonyan)

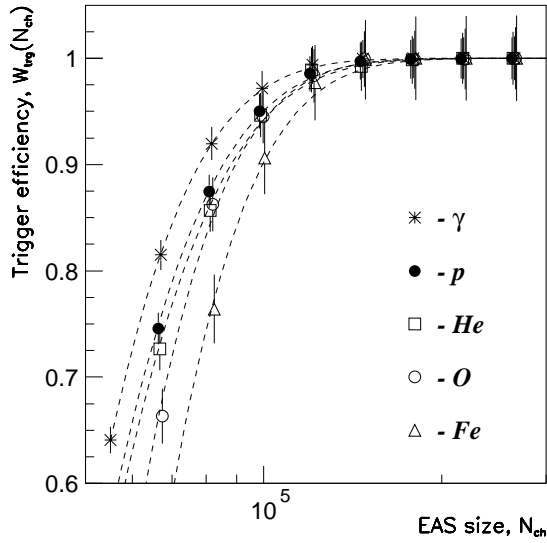


Fig. 2. Trigger efficiency of GAMMA EAS array for different primary particles. Dashed lines correspond to the exponential approximations:  $W_{trg}(A, N_{ch}) = 1 - \alpha_A \exp(-N_{ch}/N_{0,A})$ , where  $\alpha_A$  and  $N_{0,A}$  parameters depend on primary particle ( $A$ ).

$\gamma = -2.7$  [14]. Simulated samples were equal  $7.5 \times 10^5$ ,  $10^5$ ,  $7 \times 10^4$  and  $5 \times 10^4$  for  $p, He, O, Fe$  nuclei and NKG mode of CORSIKA. The samples for the EGS mode of CORSIKA were equal to  $2.5 \times 10^4$  for primary  $\gamma$ -quanta,  $7.5 \times 10^4$  for primary protons and  $3 \times 5000$  for  $He, O$  and  $Fe$  primary nuclei. The simulation strategy and reconstruction method for shower size ( $N_{ch}$ ), age parameter ( $s$ ), core coordinates ( $x_0, y_0$ ) and shower zenith angle ( $\theta$ ) were the same as in [14].

The shower trigger efficiency and shower size reconstruction errors ( $\Delta_{N_{ch}}$  and  $\sigma_{N_{ch}}$ ) are presented in Figs. 2,3 respectively. The observed differences of reconstructed shower size biases  $\Delta_{N_{ch}}$  for different primary particles (Fig. 3, lower panel) stems from differences of corresponding lateral distribution functions of shower particles.

The distribution of detected shower age parameters (GAMMA data) in comparison with expected distributions for primary  $p, He, O, Fe$  nuclei are presented in Fig. 4 (left panel). The primary elemental composition and energy spectra were taken from solution of parametrized EAS inverse problem [14] in the frameworks of the SIBYLL interaction model (Fig. 5, shaded area [14]) and were extrapolated up to the 100 TeV energy region. The reliability of this extrapolations stems from data [18].

The right panel of Fig. 4 shows distribution of shower age parameters for selected no-muon signal events (shades GAMMA data area) in comparison with corresponding expected distributions from the simulated  $\gamma$ -showers and background proton showers. It is well seen, that the EAS age parameter is also a data carrier about primary particle ( $\gamma$ -showers are younger).

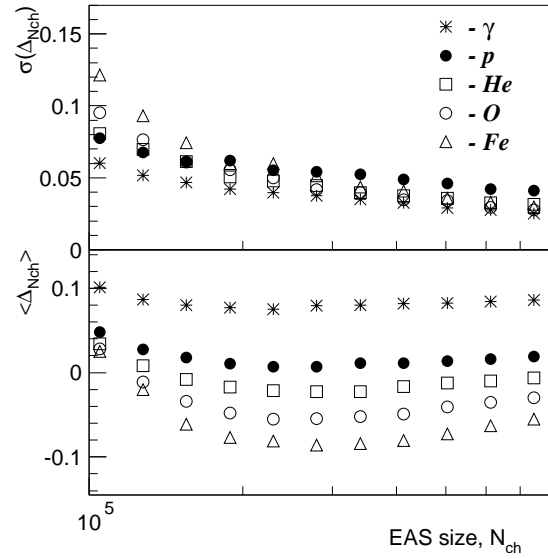


Fig. 3. Expected reconstruction error (upper panel) and average bias (lower panel) of shower size ( $N_{ch}$ ) for different primary particles (symbols).  $\Delta_{ch} = \ln(N_{ch}^*/N_{ch})$  and  $N_{ch}^*$  is an estimation of shower size  $N_{ch}$ .

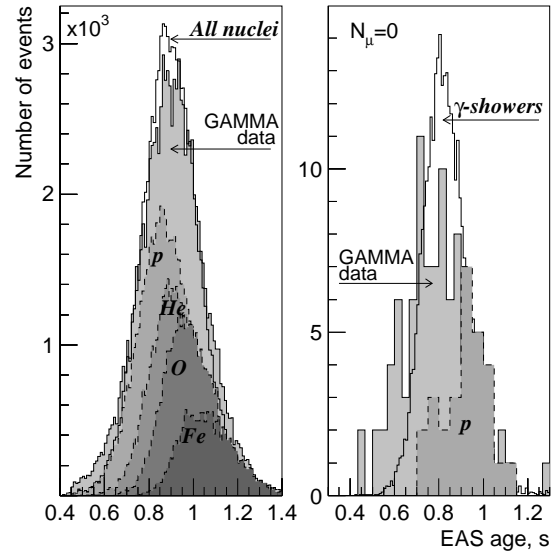


Fig. 4. Shower age parameter ( $s$ ) distribution for all showers (left panel) and no-muon detected showers ( $N_{\mu} = 0$ , right panel). Simulated data for the primary mixed composition (*All nuclei*, left panel) and primary gamma ray (right panel) are normalized to the corresponding GAMMA experimental data.

However, we did not include yet the age parameter in the  $\gamma$ -showers selection criteria. Results in Fig. 4 we use only as indication of an agreement between simulated and corresponding detected distributions.

The detected muon number spectra in the normalization of probability density function for different shower size thresholds ( $N_{ch} > 10^5, 2 \times 10^5$  and  $4 \times 10^5$ ) are presented in Fig. 6 (hollow symbols) in comparison with the corresponding expected spectra from different primary particles ( $\gamma, p, He, O, Fe$ ) and

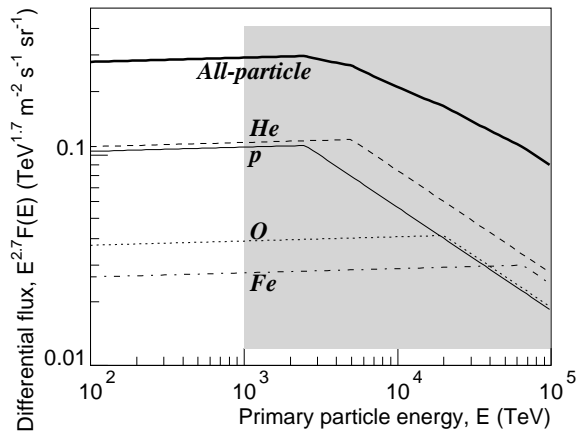


Fig. 5. Primary energy spectra and all-particle energy spectrum taken from [14] (shaded area) and corresponding extrapolations to the 100 TeV energy region.

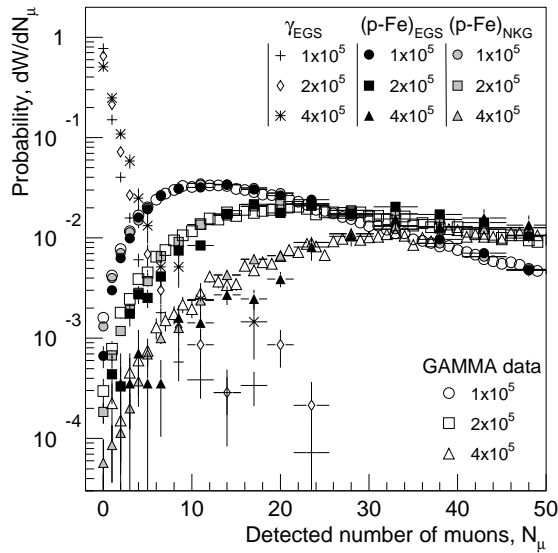


Fig. 6. Normalized detected muon number ( $N_\mu$ ) spectra for different shower size thresholds ( $10^5, 2 \times 10^5, 4 \times 10^5$ ). Hollow symbols (circle, square and triangle) are GAMMA experimental data. The symbols in  $\gamma_{EGS}$ ,  $(p-Fe)_{EGS}$  and  $(p-Fe)_{NKG}$  columns correspond to simulated data for the primary  $\gamma$  and mixed composition ( $p, He, O, Fe$  [14]) computed using the EGS and NKG modes of CORSIKA.

different simulation modes (NKG, EGS) of CORSIKA. Energy spectra and elemental composition of primary nuclei (Fig. 5) used in the Figs. 4,6 were taken from [14] and applied for the energy region  $E > 100$  TeV.

#### A. Energy estimation

The energy of primary particle is estimated using event-by-event method [15] according to the empirical expression:  $\ln E_A = A_1 \ln N_{ch} + A_2 / \cos \theta + A_3$ , where  $E$  is in GeV, parameters  $A_1, A_2$  and  $A_3$  are determined using goodness-of-fit test for simulated database and depend on primary particle  $A$ .

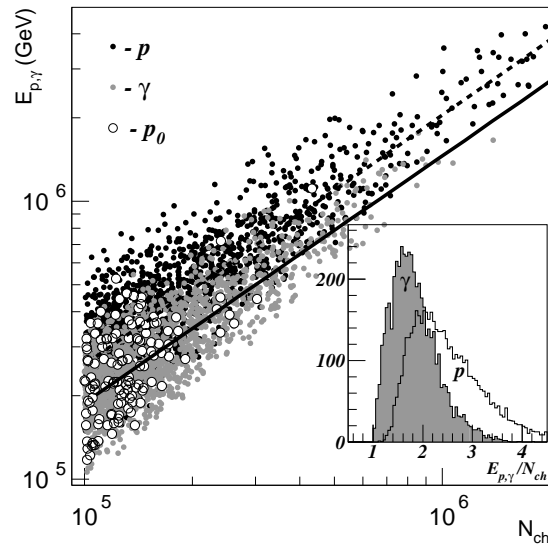


Fig. 7. Primary energy ( $E$ ) and corresponding shower size ( $N_{ch}$ ) distributions at observation level for 5000 primary protons (bold dot symbols) and 5000  $\gamma$  (gray dot symbols). Hollow circles correspond to the proton showers with no-muon signal from underground muon carpet ( $N_\mu = 0$ ). Solid and dashed lines are the log-linear approximations (see text) for primary  $\gamma$  and  $p$  correspondingly. Inset histograms are  $E_{p,\gamma}/N_{ch}$  distributions for primary proton and  $\gamma$  (shaded area).

The corresponding accuracies providing for  $\chi^2 \simeq 1$  is described by the log-linear functions  $\sigma(E_A) = \varepsilon_A - \delta_A \ln(E_A/10^5)$ , where  $\varepsilon \equiv 0.22, 0.30, 0.33$  and  $\delta \equiv 0.01, 0.02, 0.05$  for primary  $\gamma, p$  and proton induced no-muon detected shower ( $p_0$ ) respectively.

The primary energy reconstruction efficiencies are presented in Fig. 7 for different primary particles. The lines represent the log-linear empiric expression above for primary proton showers (dashed line) and  $\gamma$ -showers (solid line) respectively. It is seen, that the proton produced no-muon signal events (hollow circles) practically similar to  $\gamma$ -showers. The inset histogram shows the distribution of  $E_{p,\gamma}/N_{ch}$  ratio for  $p$  and  $\gamma$  primary particles respectively.

### III. GAMMA RAY FLUX

98000 shower events were selected for operation time  $T = 3970$  h of GAMMA experiment. Number of detected shower events versus number of detected muons ( $N_\mu$ ) for different shower size thresholds  $N_{ch} > 10^5, 2 \times 10^5$  and  $4 \times 10^5$  are presented in Fig. 8 (histograms with shaded area). The symbols in Fig. 8 are the corresponding expected number of events simulated using the CORSIKA code for primary energy spectra [14] presented in Fig. 5. The simulations were carried out for two modes of CORSIKA to get high accuracy of simulation (EGS mode) and large simulated sample (NKG mode).

The agreement of simulated and detected muon spectra in all measurement region and lack of statistically

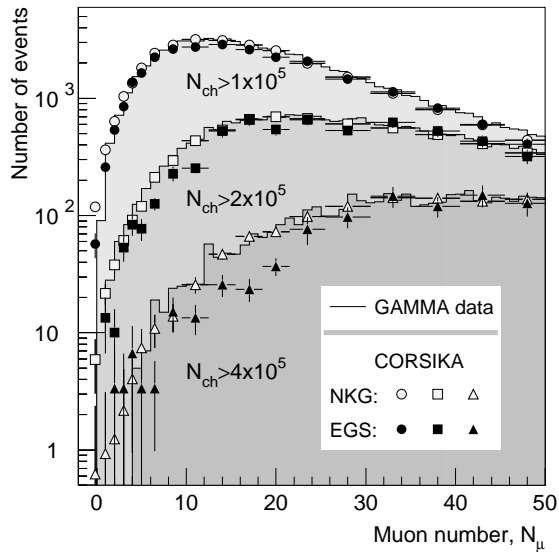


Fig. 8. Detected (histogram lines) and expected (symbols) muon number ( $N_\mu$ ) spectra for different shower size thresholds ( $10^5, 2 \times 10^5, 4 \times 10^5$ ) and different mode (NKG, EGS) of CORSIKA.

significant excess of no-muon signal events (Fig. 8) allowed us to estimate only an upper limit of  $\gamma$ -ray flux according to the expression

$$J = \frac{2\sqrt{M_0/(W_{\gamma, N_\mu=0}W_{trg, \gamma})}}{S\Omega T \cos \theta} \cdot \frac{1}{\Delta E} \quad (1)$$

where  $M_0$  is the number of no-muon detected showers,  $W_{\gamma, N_\mu=0}$  is the probability to detect no-muon signal for  $\gamma$ -showers (see Fig. 6),  $W_{trg}(E_\gamma)$  is the trigger efficiency (see Fig. 2),  $\cos \theta = 0.94$  is the average shower zenith angle,  $S$  and  $\Omega$  are the EAS core detection area and corresponding solid angle.

The obtained upper limit of differential  $\gamma$ -ray flux in the energy range 100-300 PeV are presented in Fig. 9 (black downward triangle symbol) in comparison with CASA-MIA [11], KASCADE [13] and EAS-TOP [12] data.

#### IV. CONCLUSION

An upper limit of  $\gamma$ -ray differential flux at energy  $E_\gamma \simeq 175_{-20}^{+25}$  TeV obtained with GAMMA experiment is equal to  $(5.8 - 7.0) \cdot 10^{-12} (erg \cdot m^2 \cdot s \cdot sr)^{-1}$  for 95% confidence level and it is in close agreement with the CASA-MIA data [11].

The lower limit for the primary energy spectra and elemental composition obtained with the GAMMA experiment [14] can be extended to the lower energy region up to about 100 TeV energies.

We are going to increase the underground muon carpet area up to 250 m<sup>2</sup> to improve  $\gamma$ /proton showers discrimination efficiency.

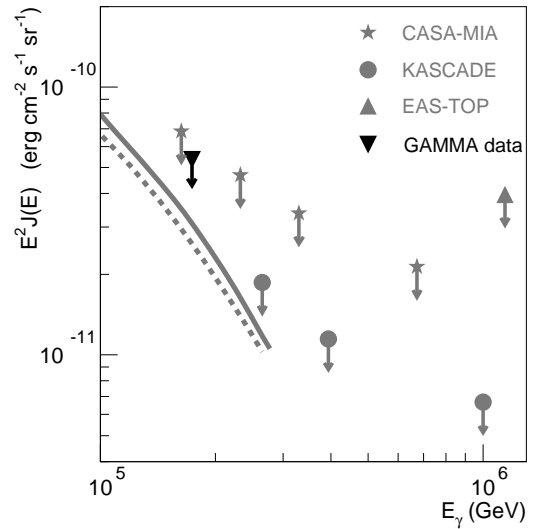


Fig. 9. Upper limit of gamma ray flux derived from detected no-muon showers (black downward triangle symbol). The gray symbols are the CASA-MIA [11], KASCADE [13] and EAS-TOP [12] data taken from [13]. The lines are expected Galactic diffuse background flux from [19].

#### V. ACKNOWLEDGMENT

This work has been partly supported by the research grant no. 090 from the Armenian government, the RFBR grant 07-02-00491 in Russia, by the Moscow P.N. Lebedev Physical Institute and the Hayastan All-Armenian Fund.

#### REFERENCES

- [1] F.A. Aharonyan, "Very High Energy Cosmic Gamma Radiation", Published by World Scientific (2004).
- [2] M. Schroedter et al., *Astrophys.J.* 634 (2005) 947.
- [3] M. Ohishi et al., *Astropart. Phys.*, 30 (2008) 47.
- [4] E. Aliu, et al., arXiv:0810.3561v1 [astro-ph] (2008).
- [5] F. Aharonian F. et al., (H.E.S.S. collaboration) *A&A*, 477, (2008) 481.
- [6] A.A. Abdo et al., *Astrophys.J.* 688 (2008) 1078.
- [7] A. Castellina et al., *Proceedings of the 27th ICRC, Hamburg, Germany* (2001) 2735.
- [8] A.M. Anokhina et al., *Astrophysics and Space Science*, 209, 1 (1993) 19.
- [9] S.I. Nikolsky, J.N. Stamenov, S.Z. Ushev, 1984, *JETP (Journal of Experimental and Theoretical Physics)*, 60, 10.
- [10] P.K. Mohanty, S.K. Gupta et al., 29th ICRC, Pune 6 (2005) 21.
- [11] Chantell, M. C. et al. 1997, *Phys. Rev. Lett.* 79, 1805./ A. Borione et al., *Astrophys. J.*, 493:175-179 (1998).
- [12] Aglietta, M. et al. 1996, *Astropart. Phys.*, 6, 71.
- [13] G. Schatz et al., *Proc. 28<sup>th</sup> ICRC*, Tsukuba (2003) 2293.
- [14] A.P. Garyaka, R.M. Martirosov, S.V. Ter-Antonyan et al., *Astropart. Phys.*, 28, 2 (2007) 169/ arXiv:0704.3200v1 [astro-ph].
- [15] A.P. Garyaka, R.M. Martirosov, S.V. Ter-Antonyan et al., *J of Phys., G: Nucl. and Part. Phys.*, 35 (2008) 115201/ arXiv:0704.3200v1 [astro-ph].
- [16] D. Heck, J. Knapp, J.N. Capdevielle, G. Schatz, T. Thouw, *Forschungszentrum Karlsruhe Report, FZKA 6019* (1998).
- [17] R.S. Fletcher, T.K. Gaisser, P. Lipari, T. Stanev, *Phys.Rev.* **D50** (1994) 5710.
- [18] A.A. Kochanov, T.S. Sinegovskaya and S.I. Sinegovsky, *Astropart. Phys.* 30 (2008) 219.
- [19] Aharonian, F. A., A. M. Atoyan 2000, *Astron. Astrophys.* 362, 937.